HHS Public Access

Author manuscript

Biochemistry. Author manuscript; available in PMC 2021 December 03.

Published in final edited form as:

Biochemistry. 2021 January 26; 60(3): 182–193. doi:10.1021/acs.biochem.0c00700.

Structural characterization of the interaction between α_MI-domain of the integrin Mac-1 ($\alpha_M\beta_2$) and the cytokine pleiotrophin

Wei Feng[1,†], **Hoa Nguyen**[1,†], **Di Shen**[1], **Hanqing Deng**[1], **Zhoumai Jiang**[1], **Nataly Podolnikova**[2], **Tatiana Ugarova**[2], **Xu Wang**[1,*]

[1]School of Molecular Sciences, Arizona State University, Tempe, Arizona, USA

[2]School of Life Sciences, Arizona State University, Tempe, Arizona, USA

Abstract

Integrin Mac-1 ($\alpha_M\beta_2$) is an adhesion receptor vital to many functions of myeloid leukocytes. It is also the most promiscuous member of the integrin family capable of recognizing a broad range of ligands. In particular, its ligand-binding α_MI-domain is known to bind cationic proteins/peptides depleted in acidic residues. This contradicts the canonical ligand-binding mechanism of αI-domains, which requires an acidic amino acid in the ligand to coordinate the divalent cation within the metal ion-dependent adhesion site (MIDAS) of αI-domains. The lack of acidic amino acids in the α_MI-domain-binding sequences suggests the existence of an as-yet uncharacterized interaction mechanism. In the present study, we analyzed interactions of α_MI-domain with a representative Mac-1 ligand, the cationic cytokine pleiotrophin (PTN). Through NMR chemical shift perturbation analysis, cross saturation, NOESY, and mutagenesis studies, we found the interaction between α_MI-domain and PTN is divalent cation-independent and mediated mostly by hydrophobic contacts between the N-terminal domain of PTN and residues in the α5-β5 loop of α_MI-domain. The observation that increased ionic strength weakens the interaction between the proteins indicates electrostatic forces may also play a significant role in the binding. Based on results from these experiments, we formulated a model of the interaction between α_MI-domain and PTN.

Keywords

Integrin; Mac-1; pleiotrophin; NMR

[*]**Corresponding Author** Correspondence should be addressed: Xu Wang, the School of Molecular Sciences, Arizona State University, Tempe, AZ 85283; xuwang@asu.edu.

[†]These authors contributed equally.

Author Contributions

Conceptualization, X. W. & T. U.; Methodology, X. W.; Investigation, W. F., H. N., D. S., H. D., Z. J.; Writing – Original Draft, W. F., H. D., D. S., H. D. & X. W.; Writing – Review & Editing, N. P., T. U. & X. W.; Funding Acquisition, X. W.; Supervision, X. W.

ACCESSION CODES

Backbone chemical shifts of wild type human α_MI-domain have been deposited into BMRB (accession code 27870).

ASSOCIATED CONTENT

Supporting Information

Additional Supporting figures can be found online. Figure S1. Sequences of α_MI-domain and PTN used in this study. Figure S2. Biophysical characterization of active α_MI-domain (E131 to K315). Figure S3. PTN-induced changes in the ^{15}N-HSQC spectrum of α_MI-domain. Figure S4. Buffer-induced differences in the ^{15}N-HSQC spectra of α_MI-domain and PTN. Figure S5. Effects of NaCl on PTN-induced NMR spectral changes of α_MI-domain. Figure S6. Full ^{15}N-HSQC of α_MI-domain in the presence of PTN, NTD, or CTD.

INTRODUCTION

Integrins are noncovalently-associated αβ heterodimers that mediate adhesive interactions of cells with the extracellular matrix and other cells. By connecting the actin cytoskeleton with the extracellular environment, integrins regulate numerous processes including cell migration, division, immune response, angiogenesis, and others. Integrins usually adopt an inactive conformation, which has a low affinity for their extracellular ligands and is converted into the active form by intracellular and extracellular signals [1]. A salient property of integrins is their broad ligand binding specificity, allowing them to engage various proteins that share no obvious sequence similarity. Even integrins that bind the well-known RGD adhesion motif also bind ligands that lack this sequence.

Integrin $\alpha_M\beta_2$ (Mac-1, CD11b/CD18), which belongs to the β_2 subfamily of leukocyte integrins, is the most promiscuous member of the entire integrin family with more than 40 reported protein ligands. Mac-1 is expressed on myeloid cells, such as neutrophils and macrophages, and mediates important adhesive reactions of these leukocytes during the inflammatory response, including migration, phagocytosis, degranulation, and others [2–5]. The variety and complexity of Mac-1 functions are believed to arise from its ability to recognize a multitude of structurally and functionally dissimilar ligands. The reported ligands include proteins that constitute the extracellular matrix (ECM) and many ECM-associated proteins released during the inflammatory response (a partial list is provided in ref. [6–8]). It also binds cellular receptors such as ICAM-1 [9], GPIbα [10], JAM-3 [11], and the recently identified SIRPα [12]. Furthermore, Mac-1 can bind proteases including elastase, myeloperoxidase, and plasminogen [13–15] and even non-mammalian proteins ovalbumin and keyhole limpet hemocyanin [6, 16].

Within Mac-1, a region of ~200 amino acid residues *inserted* into the α-subunit and referred to as the α_MI-domain is a principal ligand-binding site [17, 18] and as such, is responsible for the receptor's broad substrate specificity. α_MI-domain is a classical Rossmann fold composed of seven α-helices surrounding a mostly parallel β sheet [19]. A divalent cation-binding site known as MIDAS (metal ion-dependent adhesion site) is located at the apex of α_MI-domain where metals are coordinated by a conserved cluster of oxygenated residues (D140, S142, and S144) as well as two additional conserved residues, T209 and D242 [19]. Moreover, α_MI-domain has been crystallized in two conformations, known as "open" and "closed", corresponding to active and inactive functional states, respectively [19–22]. These conformations differ by a changed position of the C-terminal α7 helix [21]. In the open conformation, S142, S144, and T209 directly coordinate the divalent metal ion via their side chain hydroxyl oxygen atoms while D140 and D242 make indirect contacts via water molecules. The nature of the cation does not seem to be important as α_MI-domain has been crystallized in the open conformation in the presence of either Mg^{2+} or Mn^{2+} [19, 21, 22]. Furthermore, in the crystal, the side chain of a glutamate residue from a neighboring α_MI-domain molecule completes the coordination [19, 21, 22]. In the "closed" conformation, two serines coordinate a metal but a bond to threonine is broken and replaced by a bond to D242. Water molecules complete the coordination sphere and there is no equivalent of the exogenous glutamate. This conformer has been crystallized in the presence of Mn^{2+} [21]

but also in the absence of divalent metal ions [20]. Interestingly, although wild type α_MI-domain naturally adopts the “closed” conformation, it can be induced to adopt the “open” conformation if the protein is truncated at K315 [23].

Based on the finding that glutamate from another α_MI-domain is involved in cation coordination and the fact that MIDAS together with its surrounding surface-exposed side chains form the binding site for several ligands [22, 24–27], it has been proposed that the interaction with an acidic residue is required for integrin-ligand interactions [19]. Indeed, this ligand-binding mechanism has been shown for the interaction of human α_MI-domain with an aspartate residue in iC3b [28] and can also explain the role of metal-coordinating acidic residues in ligands of several other αI domain-containing and αI-less integrins [29–31]. However, there are notable exceptions. For instance, α_2I-domain of the collagen receptor integrin $\alpha_2\beta_1$ is known to bind a cyclic peptide composed entirely of basic amino acids [32–34], defying the common belief that at least one acidic amino acid must be present in the ligand.

The ligand binding promiscuity exhibited by Mac-1 also falls outside of the scope described by the canonical mechanism. Earlier studies have identified several cationic α_MI-domain-binding peptides derived from ligands that do not contain acidic residues [35–37]. In particular, the fibrinogen-derived peptide, TMKIIPFFNRLTIG (P2-C), served as a prototype peptide ligand for studies of promiscuous recognition of α_MI-domain [26] and studies using gene-targeted mice in which the C-terminal sequence of P2-C in fibrinogen was mutated have confirmed it as the binding site for Mac-1 [38]. Screening peptide libraries spanning the sequences of many reported Mac-1 ligands for α_MI-domain has shown that, within its ligands, α_MI-domain has a preference for sequences enriched in positively charged residues flanked by hydrophobic residues [7]. Acidic residues are largely omitted in those patterns. These studies led to the identification of a large group of cationic proteins as Mac-1 ligands. Many of these proteins, which include among others elastase [13], myeloperoxidase [14], the cathelicidin peptide LL-37 [39], and opioid peptide dynorphin-A [40], are normally sequestered within leukocytes and released during the inflammatory response to serve as alarm signals for the immune system [41, 42]. Other cationic Mac-1 ligands, such as pleiotrophin (PTN) [43] and platelet factor 4 (PF4/CXCL4) [44], are expressed at sites of tissue injury and seem to fulfill similar functions.

Despite the wealth of evidence identifying cationic ligands as Mac-1 targets, the mechanism of their binding is not clear. In this study, we analyzed the interaction of α_MI-domain with a typical cationic Mac-1 ligand, the cytokine PTN, using solution NMR spectroscopy. PTN is a cationic protein that modulates numerous physiological phenomena, including inflammation [45, 46]. PTN is unique among Mac-1-binding cationic proteins in that it binds both the active, “open” form of α_MI-domain (residues E131 to K315) and the inactive, “closed” form of α_MI-domain (residues E131 to T324). However, the inactive α_MI-domain’s affinity for PTN is significantly lower than that of the active α_MI-domain [43]. Our data show that the interaction between PTN and inactive α_MI-domain does not require divalent cations, but is sensitive to high ionic strength, pointing to electrostatic forces as a factor in binding. Chemical shift perturbation analysis, cross saturation, and NOESY experiments identified residues around the N/C-termini, especially the α5-β5 loop of α_MI-domain,

as being involved in PTN binding. Probing α_MI-domain with individual PTN domains showed the N-terminal domain of PTN (NTD) alone is sufficient to reproduce almost all the spectral perturbations induced by wild type PTN while the C-terminal domain of PTN (CTD) generated little perturbation on the NMR spectrum of α_MI-domain. This indicates the NTD is the major α_MI-domain binding site in PTN. In addition, intermolecular contacts between a leucine in PTN and backbone amide hydrogens in the α5-β5 loop of α_MI-domain were detected in NOESY. Mutagenesis of both acidic and hydrophobic amino acids in the α5-β5 loop of α_MI-domain also significantly affected PTN binding, indicating that both hydrophobic and electrostatic forces are involved in binding. These results defined precisely the interface between PTN and α_MI-domain and helped us formulate a model of α_MI-domain-PTN interactions.

Experimental Methods

Expression and purification of proteins

The open reading frames (ORF) of inactive human α_MI-domain (residues E131-T324, sequence shown in Figure S1), active α_MI-domain (E131-K315), or the mutants I265S or E268/262S were cloned into the pHUE vector [47] as a fusion protein with His-tagged ubiquitin at its N-terminus using SacII and HindIII as restriction sites. BL21(DE3) cells transformed with the expression plasmids were grown in M9 medium at 37 °C to an OD_{600} of ~ 0.8, at which point the culture was induced with 0.5 mM IPTG and harvested after overnight incubation at 23 °C. To prepare isotopically labeled proteins, $^{15}NH_4Cl$ and/or ^{13}C glucose was used in M9 media. $^{2}H/^{15}N$ labeled α_MI-domain was prepared by seeding 50 mL of D_2O M9 media containing ~ 8 g/L of ^{2}H-glucose with cells pelleted from 1 mL LB culture of the bacteria at OD_{600} of 1.0. After the 50-mL culture has reached an OD_{600} of 1.0, the culture was diluted with 250 mL of ^{2}H M9 media containing ~ 4 g/L of ^{2}H glucose. The total culture was induced and harvested as described above. $^{2}H/^{13}C/^{15}N$-labeled α_MI-domain was prepared similarly except $^{1}H/^{13}C$-labeled glucose was used. Post-induction cell cultures were pelleted and resuspended in lysis buffer (20 mM sodium phosphate, 0.5 M NaCl, 10 mM imidazole, 5% glycerol, 0.01% NaN_3) containing 1 mg/mL lysozyme and incubated for 20 minutes at room temperature. After sonication and centrifugation, the supernatant was collected and subjected to Ni-affinity chromatography using a 5-mL HisTrap column (GE Life Sciences). To elute the protein, an imidazole gradient of 35 to 500 mM was applied at a flow-rate of 3 mL/min. Eluent fractions containing the fusion proteins were exchanged into a buffer of 25 mM Tris and 100 mM NaCl, pH 8.0 and treated with 1/20 molar equivalent of His-tagged ubiquitinase USP2 catalytic core domain overnight at room temperature to cleave ubiquitin from the fusion protein [47]. To separate cleaved α_MI-domain from other proteins, the digestion mixture was passed through a second Ni-affinity column. Flow-through fractions were collected and applied to a Superdex 75 size exclusion chromatography column (GE Life Sciences) for further purification. The purity of the protein in each fraction was verified using SDS-PAGE.

PTN (sequence shown in Figure S1) expression and purification were performed according to a previously reported protocol [48]. Briefly, pET-15b vector harboring the human PTN ORF was transformed into OrigamiB(DE3) cells (Novagen, Madison, WI, USA). Cells were

grown in M9 medium at 37 °C to an OD_{600} of 0.8. 0.25 mM IPTG was added to the culture and the culture was incubated overnight at 23°C. Cells were harvested, resuspended in 20 mM Tris, pH 8.0, 200 mM NaCl buffer, treated with 1 mg/mL lysozyme and sonicated. After centrifugation, the supernatant was applied onto a 5-mL HiTrap SP HP column (GE Life Sciences) and eluted with 0.1 to 1.5 M NaCl gradient. Additional purification using a 5-mL HiTrap heparin column (GE Life Sciences) was carried out with the same salt gradient when necessary.

Individual domains of PTN were recombinantly expressed by first inserting the ORF of either the NTD (residues G1 to C57) or the CTD (residues N58 to K114) into the pHUE vector as a fusion partner for the His-ubiquitin. The constructs were expressed in OrigamiB(DE3) using a procedure similar to that of wild type PTN. Purifications of the domains were similar to that of α_MI-domain except no size exclusion chromatography was used.

NMR data acquisition

Data were collected on either Agilent 800 MHz or Bruker AVANCE 600 MHz and 850 MHz spectrometers equipped with cryo-probes. All NMR samples contained 0.1–1 mM inactive α_MI-domain in 20 mM HEPES, pH 7.4. All data were collected at 25 °C. For backbone assignment, HNCACB, HNCOCACB, HNCO, and HNCACO spectra were collected on $^{2}H/^{13}C/^{15}N$ α_MI-domain samples. In addition, $^{13}C/^{15}N$ α_MI-domain was used to collect HNCA, HNCOCA, HNCO, and HNCACO spectra. All triple resonance experiments were acquired with 1024 complex points in the ^{1}H dimension, 30 complex points in the ^{15}N dimension, and 60 complex points in the ^{13}C dimension. All ^{15}N-HSQC experiments were acquired with 1024 complex points in the ^{1}H dimension and 50 complex points in the ^{15}N dimension. Spectral widths are usually set to 15 ppm for ^{1}H and 34 ppm for ^{15}N with the carrier at 119 ppm. All NMR data were processed with NMRPipe [49] and analyzed with NMRView [50].

To probe PTN-induced chemical shift change, ^{15}N-HSQC spectra were acquired on samples containing 0.1 mM ^{15}N α_MI-domain with 0, 0.1, 0.2, 0.3, 0.4, 0.5, 0.8, 1.0, and 1.2 mM of PTN. The titration was carried out both in the presence and absence of $MgCl_2$ in 20 mM HEPES, pH 7.4. The $MgCl_2$-free titration was also repeated in 20 mM HEPES, pH 7.0, 150 mM NaCl buffer to gauge the effect of salt on the binding. To measure the affinity of the E258/262S α_MI-domain mutant for PTN, ^{15}N-HSQC spectra were acquired on samples containing 0.1 mM of the E258/262S mutant with 0, 0.1, 0.3, 0.5, 0.7, 1.0, and 1.2 mM of PTN in 20 mM HEPES, pH 7.4 buffer with no $MgCl_2$. The overall chemical shift change of each signal was quantified using the equation $\delta = [\Delta\delta_H^2 + (0.17\ \Delta\delta_N)^2]^{1/2}$, where $\Delta\delta_H$ is the chemical shift change in the amide hydrogen and $\Delta\delta_N$ is the chemical shift change in amide nitrogen [51].

To examine the effect of individual PTN domains on α_MI-domain, ^{15}N-HSQC spectra of 0.1 mM ^{15}N α_MI-domain with 0 or 0.7 mM of either wild type PTN, NTD or CTD were collected in 20 mM HEPES, pH 7.4 buffer without $MgCl_2$.

Cross saturation experiments were carried out on a sample containing 0.17 mM of $^{2}H,^{15}N$-labeled α_MI-domain and 0.7 mM of unlabeled PTN in 50 % D_2O, 20 mM HEPES, pH 7.4 buffer. During the experiment, a saturation pulse was applied to the ^{1}H channel at 0.9 ppm for 1.5 s. ^{15}N-edited NOESYHSQC experiments were carried out on 0.17 mM $^{2}H,^{15}N$-labeled α_MI-domain and 0.7 mM of unlabeled PTN in 10 % D_2O, 20 mM HEPES, pH 7.4 buffer. The NOE mixing time was 0.15 s. ^{13}C-HMQC-NOESY-^{15}N-HSQC experiments were carried out on a sample containing 0.5 mM of ^{15}N-labeled α_MI-domain and 2.5 mM of ^{13}C labeled PTN in 20 mM HEPES, pH 7.4 buffer. A mixing time of 0.15 s was used. Because there are only two signals in the spectrum, the chemical shift information was obtained by running separate 2D ^{1}H-^{1}H, ^{13}C-^{1}H, and ^{15}N-^{1}H projections of the original 4D experiment.

Quantification and statistical analysis

*K*ds were estimated by fitting chemical shift changes to ligand concentration using the one-to-one binding model implemented in the software xcrvfit (http://www.bionmr.ualberta.ca/bds/software/xcrvfit).

RESULTS

NMR analysis of the α_MI-domain structure

Similar to other NMR studies of protein-protein interactions, our strategy was to determine the PTN binding site by examining perturbations to the backbone amides of α_MI-domain. However, backbone atom chemical shifts of human α_MI-domain, both active and inactive forms, were not known. We determined chemical shifts of backbone amide nitrogens and hydrogens of inactive α_MI-domain using the traditional suite of multinuclear NMR spectroscopy experiments, including HNCA, HNCACB, CBCACONH, HNCOCA, and HNCOCACB [52]. These data allowed backbone atom chemical shifts of close to 90% of observable residues in the protein to be determined. Figure 1A shows the assigned ^{15}N heteronuclear single quantum coherence (HSQC) spectrum of inactive human α_MI-domain in the absence of Mg^{2+}. Unassigned residues are indicated in blue in Figure 1B. Many of these unassigned residues are located in the α3-α4 loop and α4 helix. Since most signals in the ^{15}N-HSQC are assigned, the unassigned residues most likely do not produce detectable signals in the ^{15}N-HSQC. Recently, an NMR study on mouse α_MI-domain was published [53]. Although the chemical shift assignments of mouse α_MI-domain are not yet available, a visual inspection of the mouse α_MI-domain ^{15}N-HSQC shows significant differences with the ^{15}N-HSQC of human α_MI-domain despite the high sequence homology between them.

To ensure our construct of α_MI-domain adopts the same conformation as that found in the crystal structure [21], we analyzed the secondary structure of the protein using chemical shift indexing (CSI), which is a reliable method for determining secondary structures using backbone chemical shift data [54, 55]. Our CSI results revealed a secondary structure arrangement that agrees well with the crystal structure of α_MI-domain [21] (Figure 1C), indicating our α_MI-domain in solution should adopt the same conformation as the crystal structure. It should also be noted that, because of α_MI-domain's low affinity for divalent cations [56], the protein was purified naturally in the metal-free state. This was reflected in

the fact that the ^{15}N-HSQC of α_MI-domain was unchanged after EDTA treatment while the addition of Mg^{2+} brought about drastic changes to the spectrum (Figures 2A and 6A).

We also attempted to study the active form of α_MI-domain, which can be prepared by truncating the domain at residue K315. This disrupts the hydrophobic packing that holds the α7 helix in place, allowing it to move away from the MIDAS [23]. However, the active α_MI-domain has a lower solubility than the inactive α_MI-domain and produced poor quality NMR spectra (data not shown). Analysis using size exclusion chromatography and circular dichroism spectroscopy showed that, although active α_MI-domain remains a monomer, its stability is significantly lower than that of inactive α_MI-domain (Figure S2). As a result, the current study focuses on the interaction between inactive α_MI-domain and PTN.

Chemical shift perturbation analysis of PTN's interactions with α_MI-domain

We first examined PTN's perturbation on the ^{15}N-HSQC spectrum of α_MI-domain at pH 7.4 (20 mM HEPES as the buffer) and without NaCl. Figure 2A shows the superimposed ^{15}N-HSQC spectra of α_MI-domain in the presence of different concentrations of unlabeled PTN under the salt-free condition. PTN produced significant chemical shift changes in many residues. In particular, residues D132, S144, K168, D242, E244, R261, E262, V264, I265, R266, H295, and E320 showed changes that are more than 1.5 standard deviations higher than the average. Most of these residues are located near the N/C termini side of α_MI-domain (Figures 2B and 2D, Table 1). Residues in the α5–β5 loop (residues R261 to I265) are especially well represented. However, three residues close to MIDAS, S144, D242, and E244, also showed significant chemical shift changes. Fitting of the chemical shift migration magnitudes to a one-to-one binding model showed the interaction *K*d ranges from 1 mM to greater than 3 mM. Figures 2C and S3 show the binding curves of several residues with large chemical shift changes. It should be noted that PTN also produced considerable decreases in signal intensities. The magnitudes of PTN-induced increases in the transverse relaxation rates of α_MI-domain backbone amide nitrogens are relatively uniform (Figure S3). This means the intensity change is most likely caused by changes in global motion, which is usually indicative of the formation of a larger complex.

Because PTN binds most of its receptors through electrostatic interactions, we also examined the interactions in buffer containing 20 mM HEPES, pH 7.0 and 150 mM NaCl to gauge whether electrostatic interactions play a role in the binding. The change in buffer condition did induce considerable changes in signal intensity as a result of changes in solvent exchange rates of amide hydrogens. Some chemical shift changes can also be seen. However, the changes are generally small enough to allow assignments of the signals and do not indicate large scale conformation changes in the proteins (Figure S4). Perturbations of PTN on the ^{15}N-HSQC of α_MI-domain in the presence of 150 mM NaCl at pH 7.0 are shown in Figure S5. In particular, PTN produced considerably smaller intensity and chemical shift changes in the presence of NaCl. This indicates the binding may be weakened by high ionic strength, implying that electrostatic interactions may play a role in the interaction.

PTN is composed of two thrombospondin type-1 repeat domains [48]. Our previous study showed either NTD or CTD alone is sufficient to induce Mac-1-dependent cell adhesion.

However, CTD induced higher adhesion rates than NTD [43]. To better define the α_MI-domain binding site on PTN, we probed α_MI-domain with individual domains. Figures 3 and S6 show ^{15}N-HSQC spectra of 0.1 mM α_MI-domain alone or in the presence of 0.7 mM of either wild type PTN, NTD, or CTD. Surprisingly, the data show that NTD alone is sufficient to produce almost all α_MI-domain spectral changes generated by wild type PTN, including perturbations to residues near MIDAS, the α5-β5 loop, and the N/C-termini. CTD produced little change in the α_MI-domain spectra (Figure 3). These data show NTD is the main α_MI-domain binding site.

NOE contacts between α_MI-domain and PTN

To identify the PTN binding site on α_MI-domain further, we also carried out cross saturation experiments [57] on perdeuterated ^{15}N-α_MI-domain and unlabeled PTN in 50 % D_2O. Cross saturation experiments take advantage of the intermolecular dipole-dipole interactions between hydrogens at the binding interface to transfer spin saturation on the ligand to nearby receptor hydrogens, allowing receptor atoms at the interface to be identified through the observation of intensity decrease. Our data showed that saturation at 0.9 ppm, which only affects PTN aliphatic hydrogens, significantly reduced the signal intensities of residues in the α5–β5 loop of α_MI-domain (Figure 4A, Table 1). This result is in agreement with the chemical shift perturbation experiment and offers additional proof that residues in the α5–β5 loop, are involved in binding PTN. In an attempt to determine unambiguous contacts between the two proteins, we carried out ^{13}C-HMQC-NOESY- ^{15}N-HSQC experiments on a sample containing ^{13}C-labeled PTN and ^{15}N-labeled α_MI-domain. The results showed there is an intermolecular NOE between HN of G263 in α_MI-domain and two PTN aliphatic hydrogens with chemical shifts of 0.95 ppm and 1.80 ppm. These PTN hydrogens are in turn bonded to ^{13}C atoms with chemical shifts of 25.5 ppm and 41.5 ppm, respectively (Figure 4B). These values closely match the side chain atoms of several leucines in PTN, raising the possibility that the interaction may also involve hydrophobic contacts.

Because of the insensitivity of the ^{13}C-HMQC-NOESY-^{15}N-HSQC experiment, we also collected a ^{15}N-edited NOESYHSQC spectrum on ^{2}H,^{15}N-labeled α_MI-domain in the presence of unlabeled PTN. An identical experiment was also collected in the absence of PTN to identify residual intramolecular NOE cross peaks that arise from incomplete deuteration. After eliminating artifactual signals, the confirmed intermolecular NOEs all came from residues in the α5–β5 loop (Figure 4C), with HNs of G263 and V264 making the strongest NOE contacts with PTN methyl groups. These data provide additional support for the critical role the α5–β5 loop plays in binding PTN.

Effects of α_MI-domain mutations on α_MI-domain-PTN interactions

To validate the NMR results above, we created two mutants of α_MI-domain. One contains the mutation I265S while the other contains mutations E258S and E262S. These mutations were chosen because their side chains are available for either hydrophobic or electrostatic interactions with PTN. Both sets of mutations produced significant changes in the spectrum of α_MI-domain, but the mutants appear to be well-folded (Figure 5). Titration of the E258S/E262S mutant with wild type PTN showed PTN continued to induce chemical shift changes in residues I265 and R266. However, the magnitudes of the changes are smaller and fitting

of the binding curves for I265 and R266 showed the *K*d of binding has increased modestly (Figure 5A). Because sufficient quantities of the I265S mutant were not available for a full multipoint titration, a two-point titration was completed to gauge the PTN-induced chemical shift changes in the mutant. It was found that the I265S mutation significantly reduced the number of perturbed residues in the spectrum. In particular, R261 and R266, two residues in the α5-β5 loop that experienced large PTN-induced chemical shift changes previously (Figure 2A), did not show any PTN-induced change in chemical shifts (Figure 5B). However, some residues in the N/C termini did show small PTN-induced chemical shift changes.

Effects of divalent cations on α_MI-domain-PTN interactions

Divalent cations such as Mg^{2+} play crucial roles in the canonical ligand binding mechanism by bridging acidic amino acids from the ligand and α_MI-domain's MIDAS. To evaluate the role Mg^{2+} plays in binding cationic ligands, we examined the effect of Mg^{2+} on the interaction of α_MI-domain with PTN. Because Mg^{2+} affinity of α_MI-domain is relatively low (*K*d ~ 1 mM) [56], MIDAS in α_MI-domain is not fully saturated at physiological Mg^{2+} concentrations. Therefore, we chose to investigate the interactions at 10 mM Mg^{2+}, which is high enough to ensure full saturation of the MIDAS.

Figure 6A shows the ^{15}N-HSQC spectra of Mg^{2+} -saturated α_MI-domain in the presence of different concentrations of PTN. The data showed Mg^{2+} had little effect on α_MI-domain's affinity for PTN. In fact, binding curves of some residues, such as I265 and R266, indicated α_MI-domain's PTN affinity was slightly lower in the presence of Mg^{2+} (Figure 6C). In addition, the magnitudes of PTN-induced chemical shift perturbations in the presence of Mg^{2+} were also smaller compared to the perturbations produced in the absence of Mg^{2+} (Figure 6B and Table 1). These results show that not only is the PTN-α_MI-domain interaction divalent cation-independent, the presence of Mg^{2+} may even weaken the interaction.

Discussion

In this study, we probed the interaction between inactive α_MI-domain and PTN using a variety of solution NMR techniques, including chemical shift perturbation, cross saturation, and NOESY. Table 1 lists the residues that were identified as being significantly perturbed by PTN. Residues on the N/C-termini side of α_MI-domain, especially residues in the α5–β5 loop, feature prominently in the table. Most of the residues in this region were perturbed in at least two of the techniques and an intermolecular NOE has been identified between residue G263 of α_MI-domain and a leucine in PTN. Surprisingly, the NTD of PTN appears to be the major site of interaction with inactive α_MI-domain because NTD alone was sufficient to produce most of the α_MI-domain spectral perturbations seen with wild type PTN. Since L32 is the only leucine in NTD, the leucine that contacts residues in the α5-β5 loop is most likely L32 of NTD. These results indicate that hydrophobic contacts may be important in the interaction between α_MI-domain and NTD of PTN. Two hydrophobic amino acids in α_MI-domain, I265 and F234, are near G263 and in a position to interact with L32 of NTD. Consistent with this hypothesis is the fact that the I265S mutation in

α_MI-domain significantly reduced PTN-induced chemical shift perturbation to the α5-β5 loop. The identification of NTD as the major binding site seems to contradict the previous observation that CTD induced more cell adhesion than NTD [43]. More investigations will be needed to reconcile the two results.

Hydrophobic interaction may not be the only factor in the interaction. Besides the α5-β5 loop and N/C-termini, residues around MIDAS also exhibited PTN-induced chemical shift changes. Both the MIDAS and the N/C termini of α_MI-domain have significant negative electrostatic potential, making them ideal sites for electrostatic interactions with cationic proteins. The fact that the α_MI-domain-PTN interactions are sensitive to the ionic strength may be a manifestation of the influence of electrostatic forces on the interaction. Similarly, the observation that the addition of 10 mM $MgCl_2$ actually decreased the affinity may also be the result of the increase in ionic strength brought about by $MgCl_2$.

These results have allowed us to formulate a model for the interaction between PTN and α_MI-domain. In particular, hydrophobic contacts between L32 of PTN and amino acids near the α5-β5 loop, including I265 and F234, likely form the core of a specific binding interface. This interaction is complemented by transient and dynamic interactions between acidic amino acids in α_MI-domain and basic clusters in PTN. Figure 7A shows a schematic illustration of this proposed model. It should be noted that this model is consistent with the conclusions of a study that identified peptides containing basic amino acids flanked by hydrophobic amino acids as the preferred ligands for α_MI-domain [7]. In addition, although the identification of the α5–β5 loop as a ligand binding site is novel to this study, a part of the α5 helix was identified previously as critical for the binding of the cationic fibrinogen peptide P2-C [8].

Experiments from this study demonstrate the interactions between α_MI-domain and PTN are divalent cation-independent. This mechanism differs significantly from the canonical ligand binding mechanism of αI-domains. The latter mechanism requires ligands to bind I-domains by coordinating a divalent cation in the MIDAS. Because of the requirement for the ligand to coordinate the metal, the presence of an acidic amino acid in the ligand is central to the canonical mechanism. However, it has long been known that peptides devoid of acidic amino acids can still bind α_2I-domain, although divalent metal was still required for unexplained reasons [33]. In contrast to these previous studies, the binding model established here requires no divalent cations and the major binding site seemed to be away from the MIDAS. It should also be noted that intermolecular electrostatic interactions that do not involve the divalent cation are also found in systems that utilize the canonical ligand binding mechanism. For example, basic residues in ICAM-1 have been shown to participate in its binding to α_LI-domain [30]. Similar observations have also been made in the interaction of iC3b with α_MI-domain [28].

The prominent role played by the residues around the N/C-termini of α_MI-domain in binding PTN and the proximity of the α5–β5 loop to the α7 helix are worth noting. The N/C-termini region is an important functional modulator. Mutations in both the N- and C-termini are known to activate Mac-1 [23, 58] and the shift of the C-terminal α7 helix away from the MIDAS is a crucial step in the activation of α I-domains. The C-terminus also

contains the important intrinsic ligand E320, which is responsible for initiating α I-domain conformation changes when chelated by the β I-domain. Other ligands are also known to bind to the N/C termini side of α_MI-domain. In particular, CD40L, a protein known to regulate the inflammatory activities of macrophages, was shown to bind to the sequence 162-EQLKKSKTL-170 in α_MI-domain, which is in the α1-β2 loop on the N/C-termini side of α_MI-domain [59]. The binding of PTN to this side of α_MI-domain may significantly affect these crucial allosteric interactions. The proximity of the PTN binding site to the α7 helix also suggests a possible explanation for why active α_MI-domain often has a higher affinity for PTN than inactive α_MI-domain. Specifically, activation of α_MI-domain involves the disruption of the hydrophobic core that holds the α7 helix in place [23]. The displacement of the α7 helix inevitably leads to the exposure of a larger hydrophobic patch close to the α5–β5 loop. This includes increased exposure of I265, which is both a part of the α5–β5 loop and of the hydrophobic core that holds the α7 helix in place. Ligands that bind the α5–β5 loop through hydrophobic interactions can potentially have stronger hydrophobic contacts as a result (Figure 7B). This may explain why active α_MI-domain can bind PTN with higher affinity.

The fact that inactive α_MI-domain binds PTN with lower affinity does not mean only active α_MI-domain can bind the ligand *in vivo*. Indeed, some ligands are known to bind the inactive form of integrin [60]. In addition, several features of PTN may enhance its interactions with inactive Mac-1 *in vivo*. In particular, PTN, especially the CTD of PTN, is an avid binder of glycosaminoglycans, a polysaccharide commonly found in the extracellular space. These interactions are known to lead to oligomerization or aggregation of PTN [61]. The resulting large multivalent aggregates would have a much higher affinity for inactive α_MI-domain as a result of increases in the avidity of interaction. Such an avidity-enhanced interaction mechanism is well characterized in several ligand-receptor systems [62, 63] and may allow Mac-1 with inactive α_MI-domains to serve as viable receptors for the ligands. The fact that PTN is immobilized on cell surfaces or in the extracellular matrix is also consistent with observations that immobilization of ligands may be necessary to provide responsive activation of integrins [64, 65]. In addition, it is widely accepted that outside-in signaling requires ligand-induced integrin clustering to activate intracellular signaling proteins such as Src and trigger the assembly of focal adhesion complexes [66, 67]. The oligomeric nature of PTN means binding of Mac-1 to PTN may facilitate clustering of Mac-1 and consequently activation of intracellular signaling.

Finally, cationic ligands that bind α_MI-domain differ significantly in their distribution of basic and hydrophobic amino acids. It remains to be seen whether other cationic ligands have the same mix of electrostatic and hydrophobic interactions with α_MI-domain as PTN.

Supplementary Material

Refer to Web version on PubMed Central for supplementary material.

ACKNOWLEDGMENTS

We thank Drs. Brian Cherry and Samrat Amin of the Magnetic Resonance Research Center at Arizona State University for use of the NMR spectrometers. The study is funded by grants from NIGMS/NIH (GM118518) to X.W. and NIHLB/NIH (HL63199) to T. U.

Funding Sources

This study is funded by grants from NIGMS/NIH (GM118518) awarded to X.W. and NIHLB/NIH (HL63199) awarded to T. U.

ABBREVIATIONS

CSI	chemical shift index
CTD	C-terminal domain
ECM	extracellular matrix
HMQC	Heteronuclear multiple quantum coherence
HSQC	heteronuclear single quantum coherence
MIDAS	metal ion-dependent adhesion site
NTD	N-terminal domain
PTN	pleiotrophin

REFERENCE

1. Li J, and Springer TA (2018) Energy landscape differences among integrins establish the framework for understanding activation, The Journal of cell biology 217, 397–412. [PubMed: 29122968]
2. Coxon A, Rieu P, Barkalow FJ, Askari S, Sharpe AH, Von Andrian UH, Arnaout MA, and Mayadas TN (1996) A novel role for the beta 2 integrin CD11b/CD18 in neutrophil apoptosis: a homeostatic mechanism in inflammation, Immunity 5, 653–666. [PubMed: 8986723]
3. Lu CF, and Springer TA (1997) The α subunit cytoplasmic domain regulates the assembly and adhesiveness of integrin lymphocyte function-associated antigen-1, Journal of Immunology 159, 268–278.
4. Prince JE, Brayton CF, Fosset MC, Durand JA, Kaplan SL, Smith CW, and Ballantyne CM (2001) The differential roles of LFA-1 and Mac-1 in host defense against systemic infection with Streptococcus pneumoniae, Journal of Immunology 166, 7362–7369.
5. Ding ZM, Babensee JE, Simon SI, Lu HF, Perrard JL, Bullard DC, Dai XY, Bromley SK, Dustin ML, Entman ML, Smith CW, and Ballantyne CM (1999) Relative contribution of LFA-1 and Mac-1 to neutrophil adhesion and migration, Journal of Immunology 163, 5029–5038.
6. Davis GE (1992) The Mac-1 and p150,95 beta 2 integrins bind denatured proteins to mediate leukocyte cell-substrate adhesion, Experimental Cell Research 200, 242–252. [PubMed: 1572393]
7. Podolnikova NP, Podolnikov AV, Haas TA, Lishko VK, and Ugarova TP (2015) Ligand recognition specificity of leukocyte integrin alphaMbeta2 (Mac-1, CD11b/CD18) and its functional consequences, Biochemistry 54, 1408–1420. [PubMed: 25613106]
8. Yakubenko VP, Lishko VK, Lam SC, and Ugarova TP (2002) A molecular basis for integrin alphaMbeta 2 ligand binding promiscuity, The Journal of biological chemistry 277, 48635–48642. [PubMed: 12377763]
9. Diamond MS, Staunton DE, de Fougerolles AR, Stacker SA, Garcia-Aguilar J, Hibbs ML, and Springer TA (1990) ICAM-1 (CD54)-a counter-receptor for MAC-1 (CD11b/CD18), Journal of Cell Biology 111, 3129–3139.

10. Simon DI, Chen ZP, Xu H, Li CQ, Dong JF, McIntire LV, Ballantyne CM, Zhang L, Furman MI, Berndt MC, and L¢pez JA (2000) Platelet glycoprotein Ibα is a counterreceptor for the leukocyte integrin Mac-1 (CD11b/CD18), Journal of Experimental Medicine 192, 193–204.
11. Santoso S, Sachs UJ, Kroll H, Linder M, Ruf A, Preissner KT, and Chavakis T (2002) The junctional adhesion molecule 3 (JAM-3) on human platelets is a counterreceptor for the leukocyte integrin Mac-1, J.Exp.Med 196, 679–691. [PubMed: 12208882]
12. Podolnikova NP, Hlavackova M, Wu Y, Yakubenko VP, Faust J, Balabiyev A, Wang X, and Ugarova TP (2019) Interaction between the integrin Mac-1 and signal regulatory protein alpha (SIRPalpha) mediates fusion in heterologous cells, The Journal of biological chemistry 294, 7833–7849. [PubMed: 30910815]
13. Cai TQ, and Wright SD (1996) Human leukocyte elastase is an endogenous ligand for the integrin CRR3 (CD11b/CD18, Mac-1, αMβ2) and modulates polymorphonuclear leukocyte adhesion, Journal of Experimental Medicine 184, 1213–1223.
14. Johansson MW, Patarroyo M, Oberg F, Siegbahn a., and Nilsson K(1997) Myeloperoxidase mediates cell adhesion via the αMβ2 integrin (Mac-1, CD11b/CD18), Journal of Cell Science 110, 1133–1139. [PubMed: 9175709]
15. Lishko VK, Novokhatny V, Yakubenko VP, Skomorovska-Prokvolit H, and Ugarova TP (2004) Characterization of plasminogen as an adhesive ligand for integrins αMβ2 (Mac-1) and α5β1 (VLA-5), Blood 104, 719–726. [PubMed: 15090462]
16. Shappell SB, Toman C, Anderson DC, Taylor AA, Entman ML, and Smith CW (1990) Mac-1 (CD11b/CD18) mediates adherence-dependent hydrogen peroxide production by human and canine neutrophils, Journal of Immunology 144, 2702–2711.
17. Diamond MS, Garcia-Aguilar J, Bickford JK, Corb¡ AL, and Springer TA (1993) The I domain is a major recognition site on the leukocyte integrin MAC-1 (CD11b/CD18) for four distinct adhesion ligands, Journal of Cell Biology 120, 1031–1043.
18. Yalamanchili P, Lu CF, Oxvig C, and Springer TA (2000) Folding and function of I domain-deleted Mac-1 and lymphocyte function-associated antigen-1, Journal of Biological Chemistry 275, 21877–21882.
19. Lee JO, Rieu P, Arnaout MA, and Liddington R (1995) Crystal structure of the A domain from the alpha subunit of integrin CR3 (CD11b/CD18), Cell 80, 631–638. [PubMed: 7867070]
20. Baldwin ET, Sarver RW, Bryant GL Jr., Curry KA, Fairbanks MB, Finzel BC, Garlick RL, Heinrikson RL, Horton NC, Kelley LL, Mildner AM, Moon JB, Mott JE, Mutchler VT, Tomich CS, Watenpaugh KD, and Wiley VH (1998) Cation binding to the integrin CD11b I domain and activation model assessment, Structure 6, 923–935. [PubMed: 9687375]
21. Lee JO, Bankston LA, Arnaout MA, and Liddington RC (1995) Two conformations of the integrin A-domain (I-domain): a pathway for activation?, Structure 3, 1333–1340. [PubMed: 8747460]
22. Li R, Rieu P, Griffith DL, Scott D, and Arnaout MA (1998) Two functional states of the CD11b A-domain: correlations with key features of two Mn 2+ - complexed crystal structures, Journal of Cell Biology 143, 1523–1534.
23. Xiong JP, Li R, Essafi M, Stehle T, and Arnaout MA (2000) An isoleucine-based allosteric switch controls affinity and shape shifting in integrin CD11b A-domain, The Journal of biological chemistry 275, 38762–38767. [PubMed: 11034990]
24. McGuire SL, and Bajt ML (1995) Distinct ligand binding sites in the I domain of integrin αMβ2 that differentially affect a divalent cation-dependent conformation, Journal of Biological Chemistry 270, 25866–25871.
25. Zhang L, and Plow EF (1999) Amino acid sequences within the α subunit of integrin αMβ2 (Mac-1) critical for specific recognition of C3bi, Biochemistry 38, 8064–8071. [PubMed: 10387051]
26. Yakubenko VP, Solovjov DA, Zhang L, Yee VC, Plow EF, and Ugarova TP (2001) Identification of the binding site for fibrinogen recognition peptide γ 383–395 within the αM I-domain of integrin αMβ2 Journal of Biological Chemistry 275, 13995–14003.
27. Rieu P, Ueda T, Haruta I, Sharma CP, and Arnaout MA (1994) The A-domain of α2 integrin CR3 (CD11b/CD18) is a receptor for the hookworm-derived neutrophil adhesion inhibitor NIF, Journal of Cell Biology 127, 2081–2091.

28. Bajic G, Yatime L, Sim RB, Vorup-Jensen T, and Andersen GR (2013) Structural insight on the recognition of surface-bound opsonins by the integrin I domain of complement receptor 3, Proceedings of the National Academy of Sciences of the United States of America 110, 16426–16431. [PubMed: 24065820]
29. Xiong JP, Stehle T, Joachimiak A, Frech M, Goodman SL, and Arnaout MA (2002) Crystal structure of the extracellular segment of integrin αvβ3 in complex with an Arg-Gly-Asp-Ligand, Science 296, 151–155. [PubMed: 11884718]
30. Shimaoka M, Xiao T, Liu JH, Yang Y, Dong Y, Jun CD, McCormack A, Zhang R, Joachimiak A, Takagi J, Wang JH, and Springer TA (2003) Structures of the alpha L I domain and its complex with ICAM-1 reveal a shape-shifting pathway for integrin regulation, Cell 112, 99–111. [PubMed: 12526797]
31. Emsley J, Knight CG, Farndale RW, Barnes MJ, and Liddington RC (2000) Structural basis of collagen recognition by integrin α2β1 Cell 101, 47–56. [PubMed: 10778855]
32. Ivaska J, Kapyla J, Pentikainen O, Hoffren AM, Hermonen J, Huttunen P, Johnson MS, and Heino J (1998) A peptide Inhibiting the collagen binding function of integrin α2 I domain, Journal of Biological Chemistry 274, 3513–3521.
33. Pentikainen O, Hoffren AM, Ivaska J, Kapyla J, Nyronen T, Heino J, and Johnson MS (1999) "RKKH" peptides from the snake venom metalloproteinase of Bothrops jararaca bind near the metal ion-dependent adhesion site of the human integrin alpha(2) I-domain, The Journal of biological chemistry 274, 31493–31505. [PubMed: 10531352]
34. Lambert LJ, Bobkov AA, Smith JW, and Marassi FM (2008) Competitive interactions of collagen and a jararhagin-derived disintegrin peptide with the integrin alpha2-I domain, The Journal of biological chemistry 283, 16665–16672. [PubMed: 18417478]
35. Mesri M, Plescia J, and Altieri DC (1998) Dual regulation of ligand binding by CD11b I domain. Inhibition of intercellular adhesion and monocyte procoagulant activity by a factor X-derived peptide, J.Biol.Chem 273, 744–748. [PubMed: 9422726]
36. Schober JM, Lau LF, Ugarova TP, and Lam SC (2003) Identification of a Novel Integrin αMβ2 Binding Site in CCN1 (CYR61), a Matricellular Protein Expressed in Healing Wounds and Atherosclerotic Lesions, Journal of Biological Chemistry 278, 25808–25815.
37. Ugarova TP, Solovjov DA, Zhang L, Loukinov DI, Yee VC, Medved LV, and Plow EF (1998) Identification of a novel recognition sequence for integrin α M β 2 within the gamma-chain of fibrinogen, Journal of Biological Chemistry 273, 22519–22527.
38. Flick MJ, Du X, Witte DP, Jirouskova M, Soloviev DA, Plow EF, and Degen JL (2004) Leukocyte engagement of fibrin(ogen) via the integrin receptor alphaMbeta2/Mac-1 is critical for host inflammatory response in vivo, JCI 113, 1596–1606. [PubMed: 15173886]
39. Lishko VK, Moreno B, Podolnikova NP, and Ugarova TP (2016) Identification of human cathelicidin peptide LL-37 as a ligand for macrophage integrin alphaMbeta2 (Mac-1, CD11b/CD18) that promotes phagocytosis by opsonizing bacteria, Res.Rep.Biochem. 2016, 39–55. [PubMed: 27990411]
40. Podolnikova NP, Brothwell JA, and Ugarova TP (2015) The opioid peptide dynorphin A induces leukocyte responses via integrin Mac-1 (alphaMbeta2, CD11b/CD18), Mol.Pain 11, 33. [PubMed: 26036990]
41. Oppenheim JJ, and Yang D (2005) Alarmins: chemotactic activators of immune responses, Current Opinion in Immunology 17, 359–365. [PubMed: 15955682]
42. Yang D, Postnikov YV, Li Y, Tewary P, de la Rosa G, Wei F, Klinman D, Gioannini T, Weiss JP, Furusawa T, Bustin M, and Oppenheim JJ (2012) High-mobility group nucleosome-binding protein 1 acts as an alarmin and is critical for lipopolysaccharide-induced immune responses, Journal of Experimental Medicine 209, 157–171.
43. Shen D, Podolnikova NP, Yakubenko VP, Ardell CL, Balabiyev A, Ugarova TP, and Wang X (2017) Pleiotrophin, a multifunctional cytokine and growth factor, induces leukocyte responses through the integrin Mac-1, The Journal of biological chemistry 292, 18848–18861. [PubMed: 28939773]

44. Lishko VK, Yakubenko VP, Ugarova TP, and Podolnikova NP (2018) Leukocyte integrin Mac-1 (CD11b/CD18, alphaMbeta2, CR3) acts as a functional receptor for platelet factor 4, The Journal of biological chemistry 293, 6869–6882. [PubMed: 29540475]
45. Ochiai K, Muramatsu H, Yamamoto S, Ando H, and Muramatsu T (2004) The role of midkine and pleiotrophin in liver regeneration, Liver international : official journal of the International Association for the Study of the Liver 24, 484–491. [PubMed: 15482347]
46. Yokoi H, Kasahara M, Mori K, Ogawa Y, Kuwabara T, Imamaki H, Kawanishi T, Koga K, Ishii A, Kato Y, Mori KP, Toda N, Ohno S, Muramatsu H, Muramatsu T, Sugawara A, Mukoyama M, and Nakao K (2012) Pleiotrophin triggers inflammation and increased peritoneal permeability leading to peritoneal fibrosis, Kidney international 81, 160–169. [PubMed: 21881556]
47. Catanzariti AM, Soboleva TA, Jans DA, Board PG, and Baker RT (2004) An efficient system for high-level expression and easy purification of authentic recombinant proteins, Protein science : a publication of the Protein Society 13, 1331–1339. [PubMed: 15096636]
48. Ryan E, Shen D, and Wang X (2016) Structural studies reveal an important role for the pleiotrophin C-terminus in mediating interactions with chondroitin sulfate, The FEBS journal 283, 1488–1503. [PubMed: 26896299]
49. Delaglio F, Grzesiek S, Vuister GW, Zhu G, Pfeifer J, and Bax A (1995) NMRPipe: a multidimensional spectral processing system based on UNIX pipes, Journal of biomolecular NMR 6, 277–293. [PubMed: 8520220]
50. Johnson BA (2004) Using NMRView to visualize and analyze the NMR spectra of macromolecules, Methods in molecular biology 278, 313–352. [PubMed: 15318002]
51. Farmer BT 2nd, Constantine KL, Goldfarb V, Friedrichs MS, Wittekind M, Yanchunas J Jr., Robertson JG, and Mueller L (1996) Localizing the NADP+ binding site on the MurB enzyme by NMR, Nature structural biology 3, 995–997. [PubMed: 8946851]
52. Cavanagh J (2007) Protein NMR spectroscopy : principles and practice, 2nd ed., Academic Press, Amsterdam; Boston.
53. Morgan J, Saleem M, Ng R, Armstrong C, Wong SS, Caulton SG, Fickling A, Williams HEL, Munday AD, López JA, Searle MS, and Emsley J (2019) Structural basis of the leukocyte integrin Mac-1 I-domain interactions with the platelet glycoprotein Ib, Blood advances 3, 1450–1459. [PubMed: 31053572]
54. Wishart DS, and Sykes BD (1994) The 13C chemical-shift index: a simple method for the identification of protein secondary structure using 13C chemical-shift data, Journal of biomolecular NMR 4, 171–180. [PubMed: 8019132]
55. Wishart DS, Sykes BD, and Richards FM (1992) The chemical shift index: a fast and simple method for the assignment of protein secondary structure through NMR spectroscopy, Biochemistry 31, 1647–1651. [PubMed: 1737021]
56. Ajroud K, Sugimori T, Goldmann WH, Fathallah DM, Xiong JP, and Arnaout MA (2004) Binding Affinity of Metal Ions to the CD11b A-domain Is Regulated by Integrin Activation and Ligands, The Journal of biological chemistry 279, 25483–25488. [PubMed: 15070893]
57. Takahashi H, Nakanishi T, Kami K, Arata Y, and Shimada I (2000) A novel NMR method for determining the interfaces of large protein–protein complexes, Nature Structural Biology 7, 220–223. [PubMed: 10700281]
58. Oxvig C, Lu C, and Springer TA (1999) Conformational changes in tertiary structure near the ligand binding site of an integrin I domain, Proceedings of the National Academy of Sciences of the United States of America 96, 2215–2220. [PubMed: 10051621]
59. Wolf D, Hohmann JD, Wiedemann A, Bledzka K, Blankenbach H, Marchini T, Gutte K, Zeschky K, Bassler N, Hoppe N, Rodriguez AO, Herr N, Hilgendorf I, Stachon P, Willecke F, Duerschmied D, von zur Muhlen C, Soloviev DA, Zhang L, Bode C, Plow EF, Libby P, Peter K, and Zirlik A (2011) Binding of CD40L to Mac-1's I-domain involves the EQLKKSKTL motif and mediates leukocyte recruitment and atherosclerosis--but does not affect immunity and thrombosis in mice, Circulation research 109, 1269–1279. [PubMed: 21998326]
60. Jokinen J, White DJ, Salmela M, Huhtala M, Kapyla J, Sipila K, Puranen JS, Nissinen L, Kankaanpaa P, Marjomaki V, Hyypia T, Johnson MS, and Heino J (2010) Molecular mechanism of alpha2beta1 integrin interaction with human echovirus 1, The EMBO journal 29, 196–208.

61. Maeda N, Fukazawa N, and Hata T (2006) The binding of chondroitin sulfate to pleiotrophin/heparin-binding growth-associated molecule is regulated by chain length and oversulfated structures, The Journal of biological chemistry 281, 4894–4902. [PubMed: 16373346]

62. Takemoto DK, Skehel JJ, and Wiley DC (1996) A surface plasmon resonance assay for the binding of influenza virus hemagglutinin to its sialic acid receptor, Virology 217, 452–458. [PubMed: 8610436]

63. Valverde P, Delgado S, Martinez JD, Vendeville JB, Malassis J, Linclau B, Reichardt NC, Canada FJ, Jimenez-Barbero J, and Arda A (2019) Molecular Insights into DC-SIGN Binding to Self-Antigens: The Interaction with the Blood Group A/B Antigens, ACS chemical biology 14, 1660–1671. [PubMed: 31283166]

64. Li J, and Springer TA (2017) Integrin extension enables ultrasensitive regulation by cytoskeletal force, Proceedings of the National Academy of Sciences of the United States of America 114, 4685–4690. [PubMed: 28416675]

65. Schurpf T, and Springer TA (2011) Regulation of integrin affinity on cell surfaces, The EMBO journal 30, 4712–4727. [PubMed: 21946563]

66. Abram CL, and Lowell CA (2009) The ins and outs of leukocyte integrin signaling, Annual review of immunology 27, 339–362.

67. Legate KR, Wickstrom SA, and Fassler R (2009) Genetic and cell biological analysis of integrin outside-in signaling, Genes & development 23, 397–418. [PubMed: 19240129]

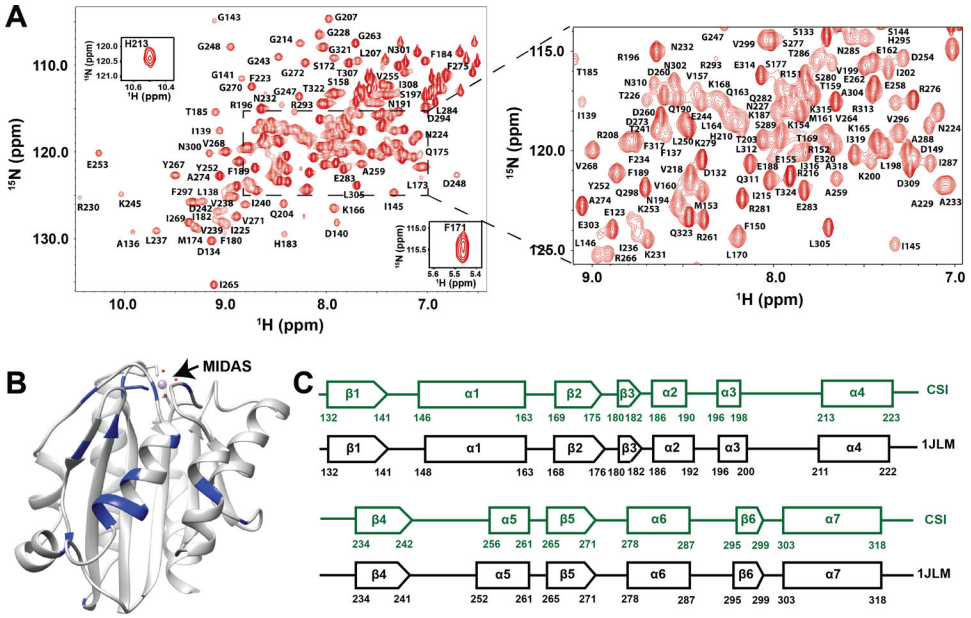

Figure 1.

NMR analysis of wild type α_MI-domain structure. A) Assigned ^{15}N-HSQC spectrum of inactive α_MI-domain (E131-T324). B) Ribbon representation of α_MI-domain crystal structure (PDB accession code: 1JLM) with unassigned residues colored in blue. C) Comparison of secondary structures of α_MI-domain derived from NMR chemical shift index (CSI) analysis and the crystal structure 1JLM.

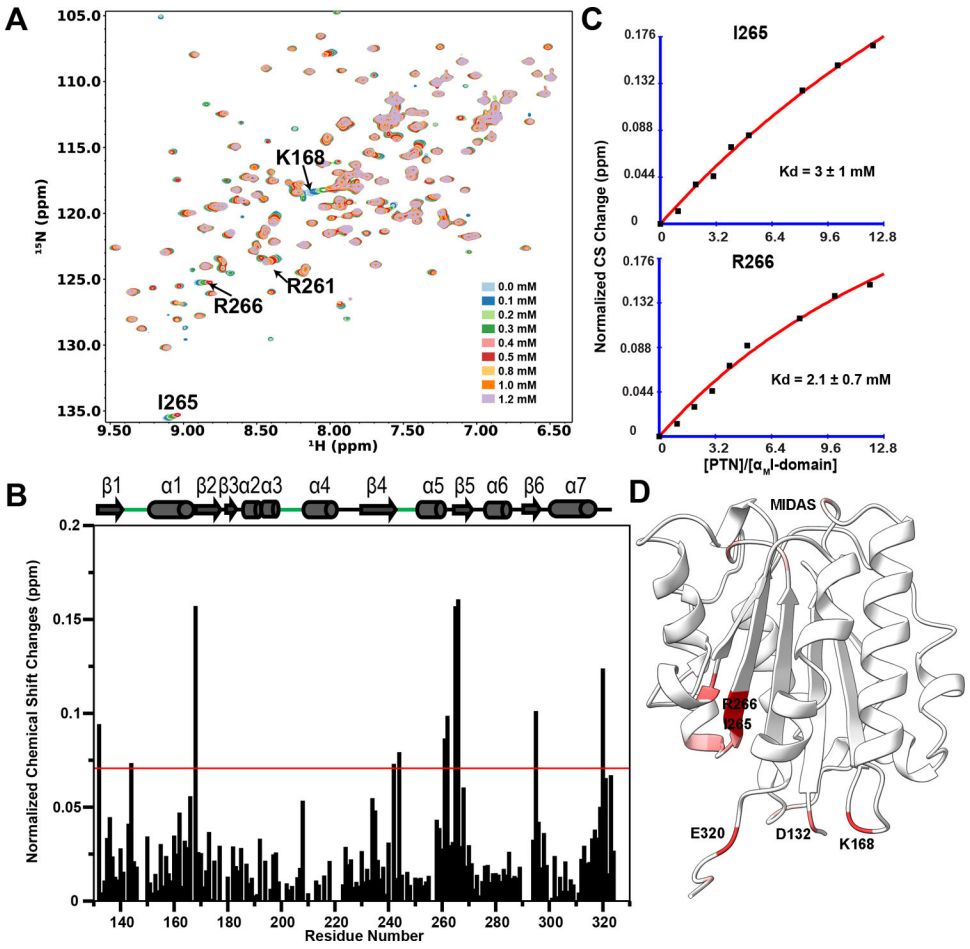

Figure 2.

PTN-induced changes in the ^{15}N-HSQC spectrum of α_MI-domain. A) Superimposition of ^{15}N-HSQC spectra of α_MI-domain at different PTN concentrations (see color legend for PTN concentrations). B) Residue specific chemical shift changes induced by 1.2 mM PTN. Data are derived from spectra shown in (A). The value of 1.5 standard deviations higher than the average chemical shift change is indicated by the red line. C) Binding curves deduced from PTN-induced changes in the chemical shifts of I265 and R266 backbone amide signals. *K*d was calculated by fitting the curves using a one-to-one binding model. D) Ribbon representation of α_MI-domain with PTN-induced chemical shift change of each residue indicated by a white-to-red color gradient covering the range 0.05 (white) to 0.15 (red) ppm.

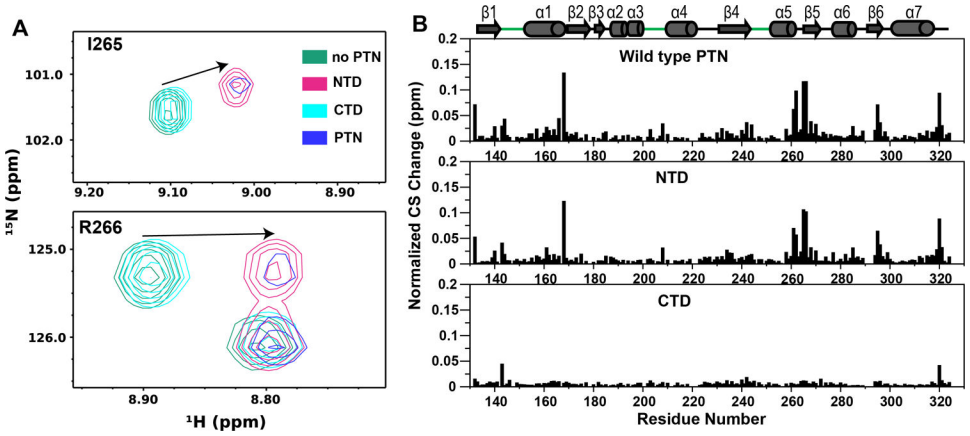

Figure 3.

Interactions of α_MI-domain with PTN domains. A) Sections from ^{15}N-HSQCs of 0.1 mM α_MI-domain alone (green) or in the presence of 0.7 mM of either NTD (purple), CTD (cyan), or wild type PTN (blue). Note that the signal for I265 was aliased in the ^{15}N dimension. B) Comparisons of the magnitudes of backbone amide chemical shift changes induced by wild type PTN, NTD, and CTD.

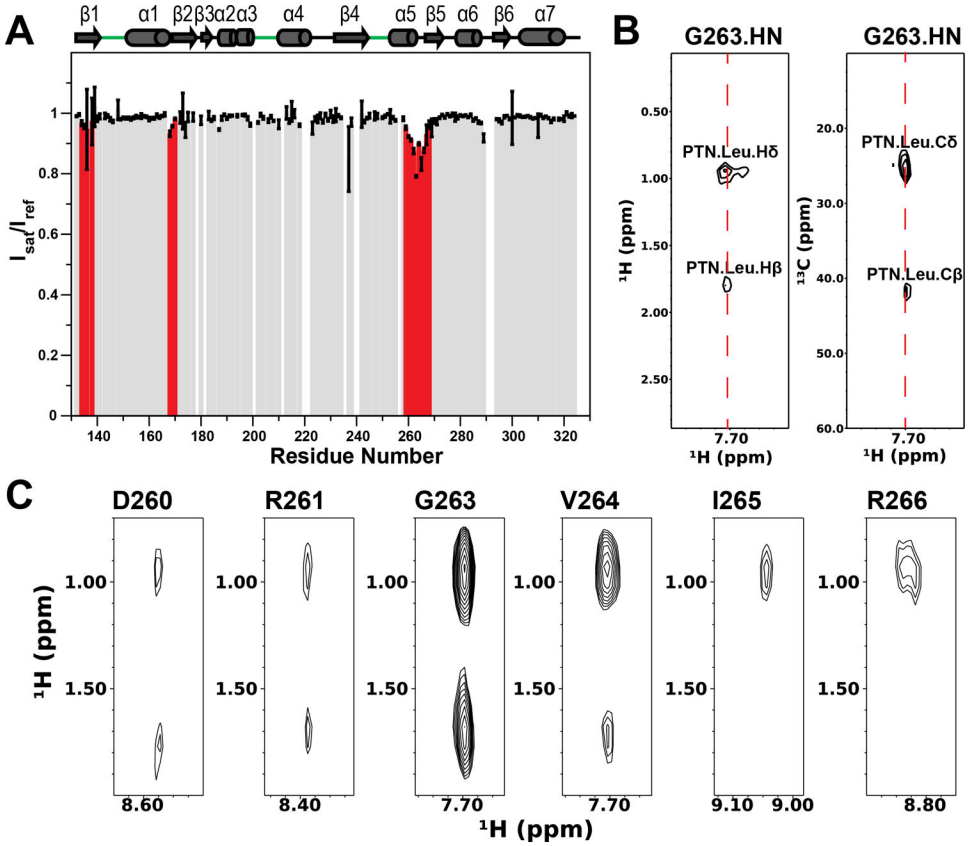

Figure 4.

Contacts between α_MI-domain and PTN. A) Signal intensity ratios of ^{2}H,^{15}N-α_MI-domain with (Isat) and without (Iref) PTN saturation. Residues in the α5–β5 loop of α_MI-domain are highlighted in red. Secondary structures of α_MI-domain as well as segments forming the MIDAS (in green) are indicated on top of the chart. B) Strips from the ^{13}C-HMQC-NOESY-^{15}N-HSQC experiment showing contacts between G263.HN of α_MI-domain (7.70 ppm) and Leu Hδ and Hβ of PTN (0.95 and 180 ppm). C) Strips from ^{15}N-edited NOESYHSQC spectrum of ^{2}H,^{15}N-labeled α_MI-domain in the presence of PTN. Contacts are observed only between HN of residues in the α5–β5 loop and PTN.

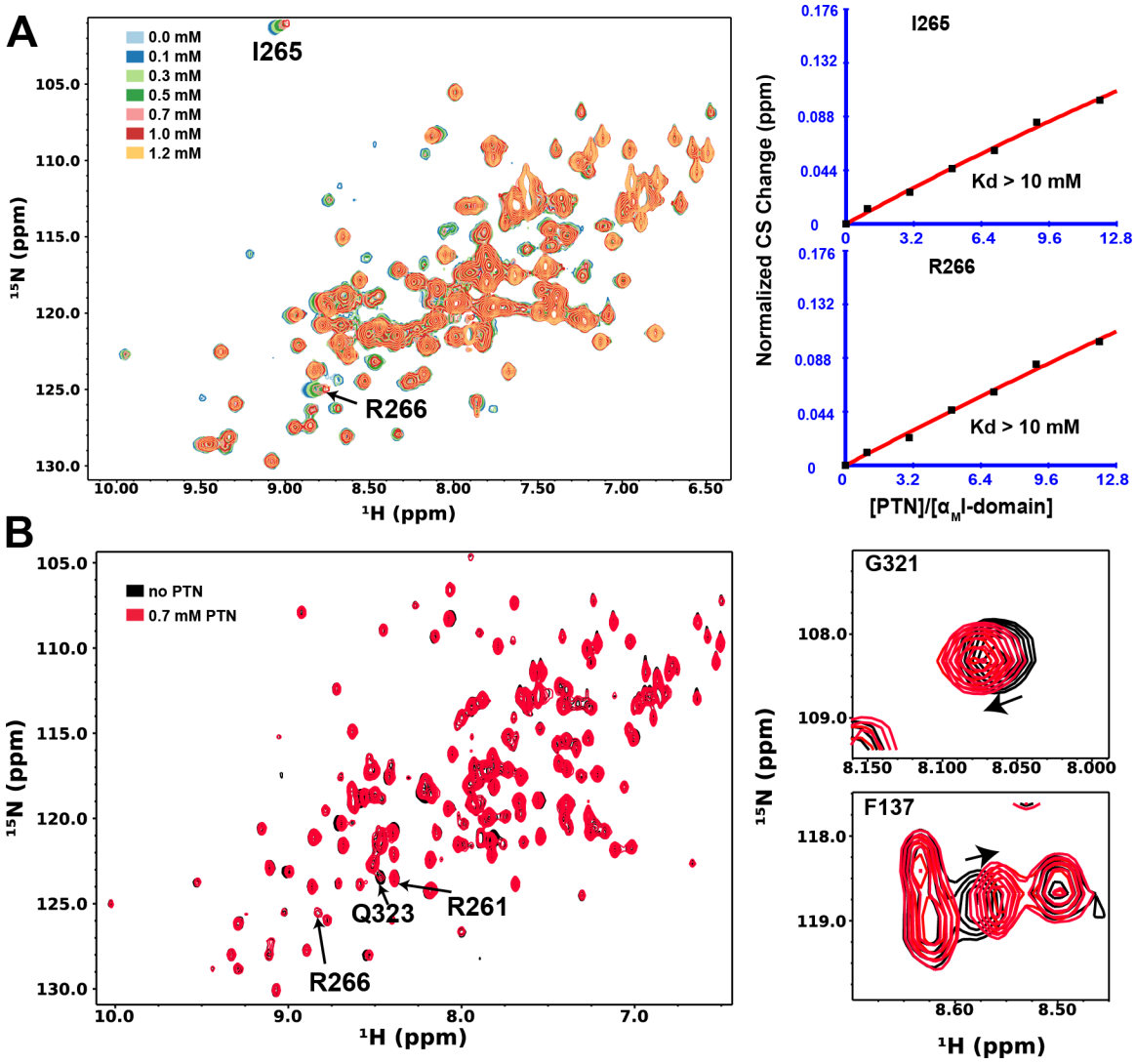

Figure 5.

Effects of α_MI-domain mutations on its interactions with PTN. A) ^{15}N-HSQC spectra of 0.1 mM E258S/E262S α_MI-domain mutant in the presence of different concentrations of PTN (see color legend for PTN concentrations). Note the signal for I265 was aliased in the ^{15}N dimension. Binding curves for residues I265 and R266 are shown on the right. B) ^{15}N-HSQC spectra of 0.1 mM I265S α_MI-domain mutant in the presence of 0.7 mM PTN. Details of spectral perturbations of some identifiable N/C termini residues are shown on the right.

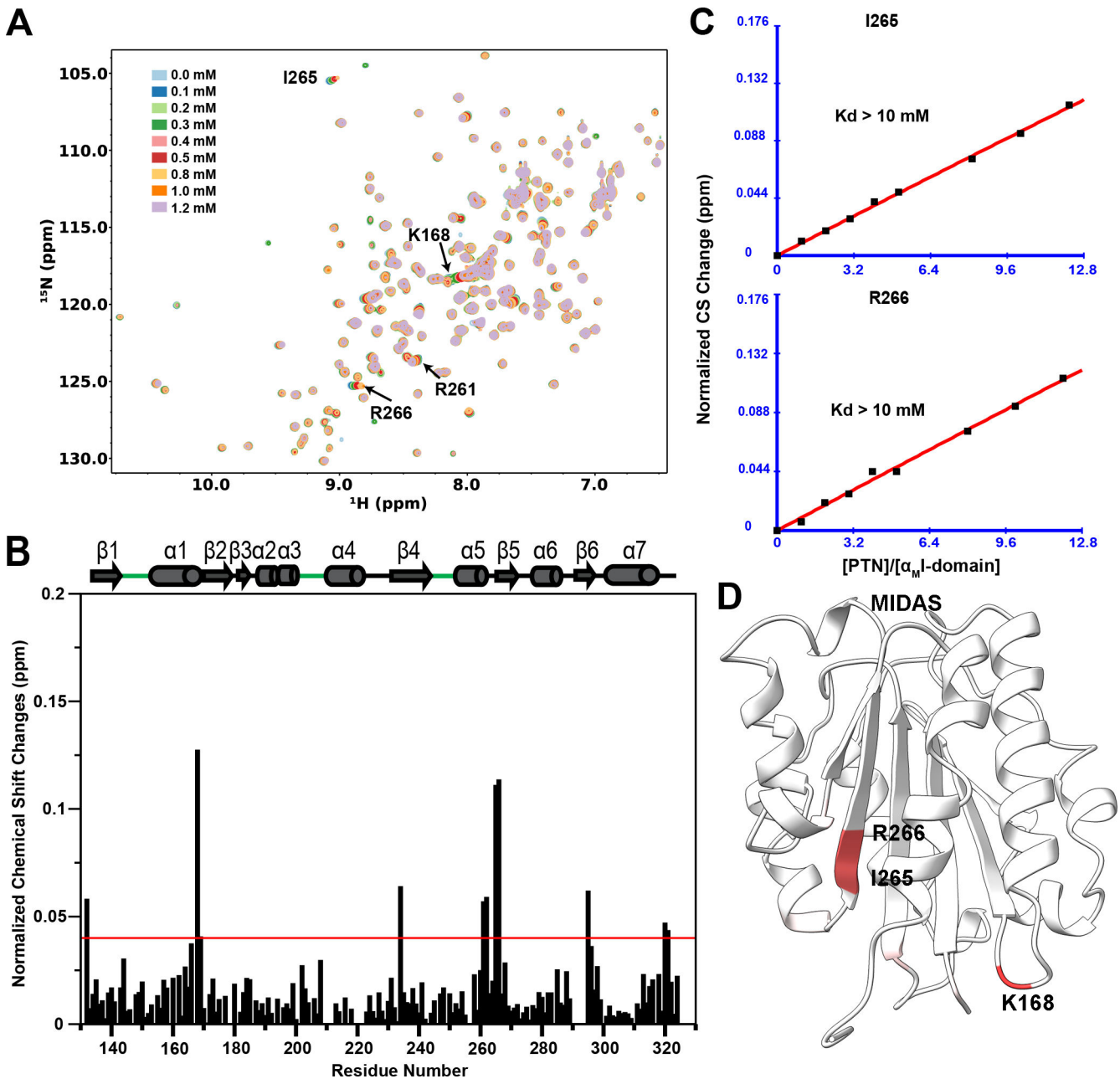

Figure 6.

Effects of Mg^{2+} on PTN-induced chemical shifts in α_MI-domain. A) ^{15}N-HSQC spectra of α_MI-domain at different concentrations of PTN (see color legend for PTN concentrations). B) Residue specific chemical shift changes induced by 1.2 mM PTN. Data are derived from spectra shown in (A). The value of 1.5 standard deviations higher than the average change is indicated by the red line. C) Binding curves derived from chemical shift changes and intensity changes of residues I265 and R266 of α_MI-domain. D) Ribbon representation of α_MI-domain with PTN-induced chemical shift change of each residue indicated by a white-to-red color gradient covering the range 0.05 (white) to 0.15 (red) ppm.

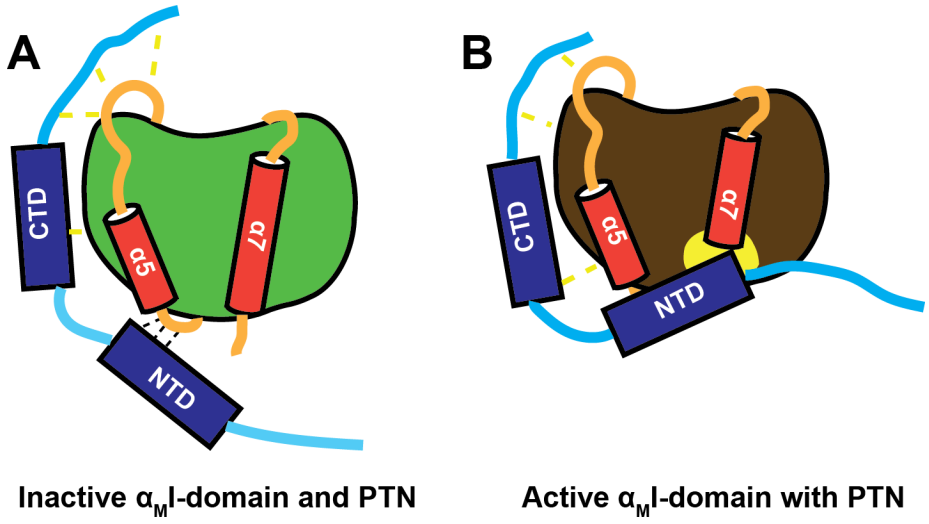

Figure 7.

Schematic model of α_MI-domain-PTN interactions. A) Inactive α_MI-domain (green) interacts with PTN's NTD (blue) through hydrophobic interactions mediated by its α5-β5 loop. Transient electrostatic interactions (yellow lines) between other domains of PTN and MIDAS of α_MI-domain are also possible. B) Active α_MI-domain (brown) has an extra hydrophobic patch (yellow) due to the truncation of the α7 helix, allowing it to have stronger hydrophobic interactions with PTN.

Table 1.

Summary of major PTN-induced perturbations in the backbone amide signals of α_MI-domain. Values are only shown if chemical shift perturbations are more than 1.5 standard deviations above average, or cross saturation intensity ratios are less than 90 %.

Residue number	Technique			
	CS Change[1] (ppm)		Cross Saturation (I_{sat}/I_{ref})	NOESY
	0 mM Mg^{2+}	10 mM Mg^{2+}		
D132	0.094	0.058		
S144	0.073			
K168	0.157	0.147		
F234		0.064		
D242	0.073			
E244	0.079			
R261	0.086	0.056	0.879 ± 0.004	NOE to PTN
E262	0.098	0.058		
G263			0.745 ± 0.003	NOE to PTN
V264	0.097		0.826 ± 0.005	NOE to PTN
I265	0.157	0.111	0.751 ± 0.029	NOE to PTN
R266	0.160	0.113	0.877 ± 0.007	NOE to PTN
H295	0.100	0.062		
E320	0.123	0.047		
G321		0.043		

[1]Chemical shift perturbation is calculated using the formula $\sqrt{\Delta H^2 + (0.17 * \Delta N)^2}$.